Observation of S^* production at 1.98 GeV/c †

M. Buttram,‡ H. B. Crawley, D. W. Duke,‖ R. C. Lamb, R. J. Leeper, and F. C. Peterson
Ames Laboratory–ERDA and Department of Physics, Iowa State University, Ames, Iowa 50010
(Received 28 August 1975)

We have studied the S^* meson using data from the reactions $\pi^- p \to \pi^+\pi^- n$ and $\pi^- p \to K^+K^- n$ at 1980 MeV/c. The parameters of the S^* pole were found by fitting the dimeson mass spectra from these reactions to a Breit-Wigner resonance formula with a coherent background. The dimeson mass was calculated from the beam and neutron four-vectors, the latter being measured by a time-of-flight technique. The mass resolution is $\sigma = 4$ MeV/c^2. Dimeson production was identified by analyzing the final-state meson trajectories with a magnetostrictive wire spark-chamber spectrometer. The events in our data sample were required to have a slow forward-going neutron which restricted the allowed range of four-momentum transfers to $|t - t_{\min}| < 0.003$ (GeV/c)^2 in the S^* region. From a sample of 21 700 $\pi^+\pi^- n$ events and 52 $K^+K^- n$ events, we find the position of the S^* pole to be $(970 \pm 5) - i(22 \pm 5)$ MeV/c^2 as compared to the present world average value of $(993 \pm 4) - i(20 \pm 4)$ MeV/c^2.

I. INTRODUCTION

Both the rapid drop in the cross section for the process

$$\pi^- p \to \pi^+\pi^- n \tag{1}$$

near dipion mass 950 MeV/c^2 and the rapid rise above threshold for the reaction

$$\pi^- p \to K^+K^- n \tag{2}$$

have been explained in terms of a pole in the $\pi\pi$ scattering amplitude near K^+K^- threshold.[1] This pole, known as the S^*, has been shown to occur in the dipion s-wave.[2] The study of this resonance typically has proceeded either through a fit of a Breit-Wigner resonance form to the mass spectra for dimeson-production reactions[3-4] or through a complete partial-wave analysis.[5-6] A primary advantage of the full partial-wave analysis is its use of angular information to separate the s-wave contribution to the cross section from the contributions of higher partial waves. For the purpose of studying the S^* these higher partial waves may be considered a background. The largest such background typically comes from the ρ resonance in the p wave although the d wave has also been shown to be important.[5]

In this paper we present data on reactions 1 and 2 from an experiment which studied the reaction

$$\pi^- p \to X^0 n \tag{3}$$

at a beam momentum of 1980 MeV/c. Here X^0 stands for any nonstrange neutral meson system. As will be discussed below, the neutron from reaction (3) was experimentally chosen to be in the forward direction and of relatively low momentum. In the over-all center-of-mass frame such neutrons are produced very near to 180° from the incident beam direction. The events accepted were, therefore, extremely peripheral corresponding to four-momentum transfers squared in the range $|t - t_{\min}| < 0.003$ (GeV/c)^2 for X^0 masses below 1000 MeV/c^2. The minimum momentum transfer $t_{\min}$ is, of course, a function of the X^0 mass.

As has been noted previously the ρ-production differential cross section dips near $t = t_{\min}$.[5] As a result, we observe very little ρ production in our data and the S^* becomes its dominant feature. This combined with the relative sharpness of the S^* effect allows a precise determination of the S^* parameters without any attempt at partial-wave separation.

II. EXPERIMENTAL DETAILS

The apparatus used in this experiment has been described before[7] and will be discussed in detail elsewhere. The data were taken at the Argonne National Laboratory Zero Gradient Synchrotron (ZGS). At beam momentum 1980 MeV/c, a typical beam flux was 2×10^5 particles per pulse in a ± 1.5% momentum bite. Beam momentum was further analyzed to ± 0.25% by a set of six overlapping tagging counters at the first focus. As is shown in Fig. 1, neutrons from reaction (3) were detected after a 5.30-m flight path from the 38.1-cm liquid-hydrogen target. The neutron-counter array was built of 30 plastic scintillator detectors each 30 cm × 30 cm × 15 cm deep. The array was centered on the beam line and subtended laboratory angles up to 12.5°. The total solid angle subtended by the neutron-counter array was 0.098 sr.

As was mentioned above, the experiment was designed to detect only the most peripheral events from reaction (3). These events correspond to slow forward-produced neutrons where slow means

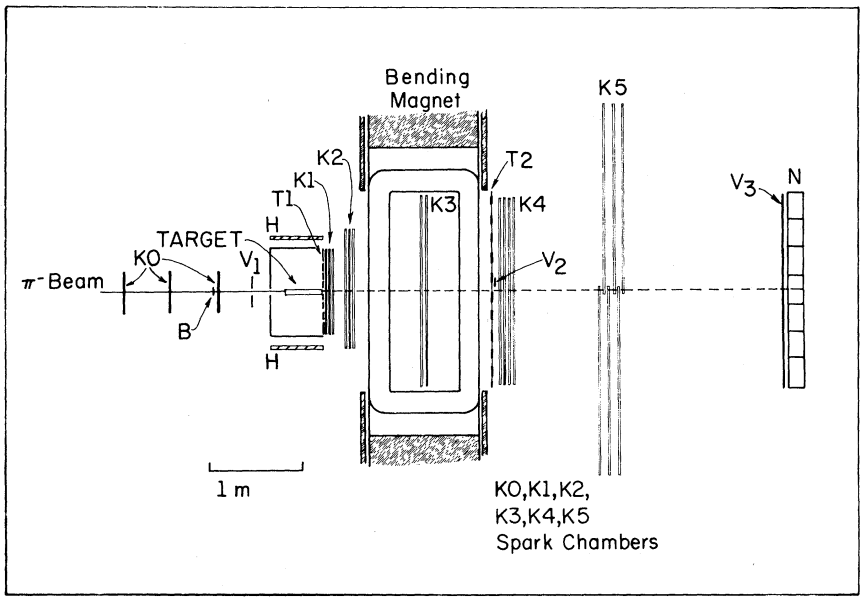

FIG. 1. Plan view of the experimental apparatus including the beam and trigger counters, the neutron detector (N), and the spectrometer.

neutron speed $\beta = v/c$ in the range 0.17 to 0.42. For our 5.30-m flight path the corresponding neutron time-of-flight (TOF) interval is 42 to 103 nsec. The mass of the X^0 in reaction (3) may be calculated from the beam and neutron four-momenta. In the forward direction this calculated mass, the missing mass (MM), is a strong function of TOF, but a very slowly varying function of the neutron polar angle. Thus, there is nearly a one-to-one correspondence between the measured TOF and MM. For the TOF range of this experiment, the MM lies in the interval 760 to 1080 MeV/c^2. The MM resolution is also most strongly dependent on the TOF resolution. Even with our relatively large 30-cm neutron counters, our TOF resolution $\sigma = 0.6$ nsec makes the principal contribution to the calculated MM resolution which is $\sigma = 4$ MeV/c^2 at an X^0 mass of 950 MeV/c^2.

The momentum and angle measurements required to select events from reactions (1) and (2) were made by incorporating the neutron detection apparatus into the effective mass spectrometer[8] (EMS) at the ZGS. The EMS is a magnetostrictive wire spark-chamber spectrometer with a typical spatial resolution of 0.5 mm and a magnetic field integral of 1140 kG cm. Its over-all momentum resolution is $\Delta p/p = 0.002p$ in units of GeV/c. This corresponds to an effective mass resolution for the pion pair of reaction 1 of 6 MeV/c^2 at an effective mass of 950 MeV/c^2.

The experimental logic was designed for maximum flexibility in detecting all the final states of the X^0 in reaction (3) subject to the constraints imposed by the spectrometer. A specific spectrometer requirement was at least one particle through all five spark-chamber planes. This was implemented by requiring at least one charged particle in the 40-element $T2$ hodoscope following the magnet. The additional logic requirements were a beam particle signal, one and only one neutron counter signal during the allowed TOF interval, and at least one particle in the 11-counter hodoscope $T1$ between the target and $K1$ chambers. An event was vetoed if a charged particle hit the beam halo counter $V1$, the unreacted beam veto counter $V2$, or that element of the charged-particle veto hodoscope $V3$ which covered the counter which detected the neutron. To avoid timing ambiguities, any event which had another beam particle arrive within 400 nsec of the triggering beam particle was eliminated.

Events from reaction (3) were subdivided into three analyzable classes depending upon the amount of spectrometer information available. The first class of events had two charged particles of opposite polarity momentum analyzed in the spectrometer. For reactions (1) and (2), these events were four-constraint (4C). The cuts used to select the final data sample of four-constraint events for reactions (1) and (2) required that the longitudinal momentum balance to ± 7 MeV/c, that the two transverse momentum components balance to ± 4 MeV/c, and that the mass squared of the neutron as calculated from the beam and meson

four-vector be correct to ± 0.05 $(\mathrm{GeV}/c^2)^2$.

For the second class of events, one particle trajectory was momentum-analyzed and a second had its angles measured in the front EMS spark chambers $K1$ and $K2$. For reactions (1) and (2) such events are three-constraint (3C), the specific constraints used being coplanarity, meson-meson opening angle, and the momentum of the analyzed trajectory. Coplanarity was defined as the tilt angle between the two planes formed by the π^+ and X^0 directions and by the π^- and X^0 directions. The X^0 direction is along the vector difference between the beam and neutron momenta. The coplanarity angle was required to be less than $\pm$ 80 mrad. The coplanarity constraint is a requirement of three-momentum conservation which means that it is independent of any final-state mass assignments. The opening angle between the mesons may also be calculated from three-momentum conservation. Agreement between the measured and calculated opening angles was required to within $\pm$ 50 mrad. Finally, energy conservation plus an explicit choice of masses can be used to predict the momentum of the measured trajectory. The difference between measured and predicted momenta divided by the predicted momentum was required to be less than $\pm$ 0.04.

Events of the third class had one momentum-analyzed track and no further spectrometer information. For reactions (1) and (2) they are one-constraint (1C), the constraint used being the momentum-difference constraint described above for 3C events. Additional counter data were also used with 1C events from reactions (1) and (2) to reduce their signal-to-noise ratio. The second meson was required to have been detected either in the $T1$ counters or in the 16-counter hodoscope H which surrounded the target on its remaining five sides. The specific element of $T1$ or H which should have detected the second meson was determined from momentum conservation and a signal from that counter was required for all events in the final 1C data sample. In Fig. 2 we present the momentum-difference constraint for 1C events after the counter cut. The signal-to-noise ratio for the data inside our $\pm$ 0.03 cut is 11.5-to-1.

In all, a total of 7.4×10^9 beam pions were used in the experiment described in this paper. These yielded 441 4C $\pi^+\pi^-n$ events, 52 4C K^+K^-n events, 3266 3C $\pi^+\pi^-n$ events, and 17977 1C $\pi^+\pi^-n$ events. The number 17977 includes both signal and noise. The other event samples were effectively free of noise. For reaction (2) (K^+K^-n) near threshold virtually all the data are 4C; therefore, only these data were used for analysis of the K^+K^-n final state.

Because of its small size, the 4C $\pi^+\pi^-n$ data sample was used to check spectrometer alignment only. Figure 3 presents for these events the difference between the MM and the effective mass of the meson pair. The distribution in Fig. 3 shows the agreement between the effective mass and MM scales. A two-dimensional histogram (not shown) of effective mass versus MM shows no systematic variation between the two mass scales as a function of mass. Furthermore, the width of the distribution in Fig. 3 is consistent with the stated MM and effective mass resolutions.

To verify our mass scale we look for ω production in events fitting the hypothesis $\pi^-p\to\pi^+\pi^-\pi^0n$.

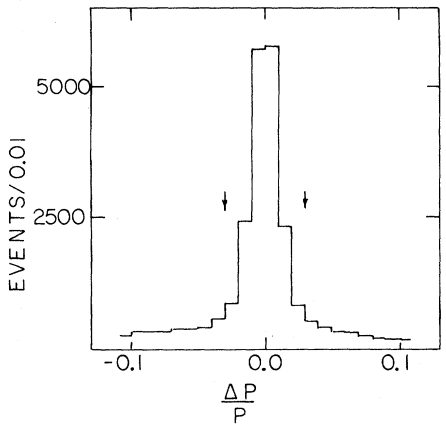

FIG. 2. For the 1C data from the reaction $\pi^-p\to\pi^+\pi^-n$, the momentum of the measured track as calculated from four-momentum conservation minus the measured momentum divided by the calculated momentum. Events in this figure were required to have a signal from the unanalyzed pion in the $T1$ or H counter (Fig. 1) predicted by three-momentum conservation. The arrows indicate the cuts used to select the final data sample.

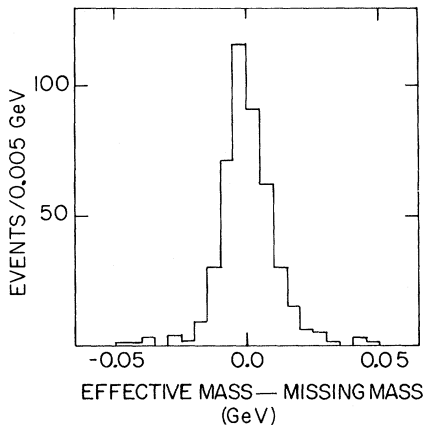

FIG. 3. The difference between the spectrometer measurement of dipion mass and the missing mass for the reaction $\pi^-p\to\pi^+\pi^-n$. The events in this figure are 4C.

Figure 4 shows an ω signal near our low mass-acceptance limit. An examination of our mass acceptance shows that it is nearly constant through the region of the figure and does not distort the ω signal. The data in Fig. 4 are fitted to a Gaussian signal plus a constant background. The width of the ω from the fit is $\Gamma = (13 \pm 3)$ MeV/c^2. After correction for our experimental resolution we find the ω natural width to be (9 ± 3) MeV/c^2 consistent with the tabulated world average.[1] The ω peak is centered at (781 ± 2) MeV/c^2 slightly below but consistent with the tabulated value of 783 MeV/c^2. As will be considered later, we have another check on the MM scale as the MM spectrum for 4C K^+K^-n events is found to be consistent within the experimental resolution with a threshold at $2m_{K^+}$.

The MM for 1C $\pi^+\pi^-n$ events is histogrammed in Fig. 5. The data show flat behavior at high and low MM with a rapid transition over the 40-MeV/c^2 interval between 940 and 980 MeV/c^2. This we identify as the S^* edge. The normally large ρ signal is not apparent even though the mass spectrum begins at 770 MeV/c^2, the maximum of the ρ peak. An examination of the events falling immediately outside the 1C $\pi^+\pi^-n$ cut shows a flat MM spectrum. Given the 11.5-to-1 signal-to-noise we expect 24 background events per 5-MeV/c^2 bin in Fig. 5.

Figure 6 presents the MM spectrum for 3C $\pi^+\pi^-n$ events. There are significantly fewer events than in the 1C spectrum and they are concentrated at low masses. However, a pronounced break is still apparent near 950 MeV/c^2.

To investigate the differences between 3C and 1C spectra we have performed a Monte Carlo calculation of the spectrometer acceptance. At discrete values of MM, events were generated to populate uniformly the neutron counters as the data were observed to do. Decay pions from the X^0, which was assumed to be spin zero, were propagated through the spectrometer and the event was assigned to a constraint class or was undetectable depending on which spark chambers intercepted the trajectories. For purposes of field integration, a square field with vertical focusing was found to be adequate after comparison with a sample of events processed using a full inhomogeneous field integration. Corrections for in-flight decays were

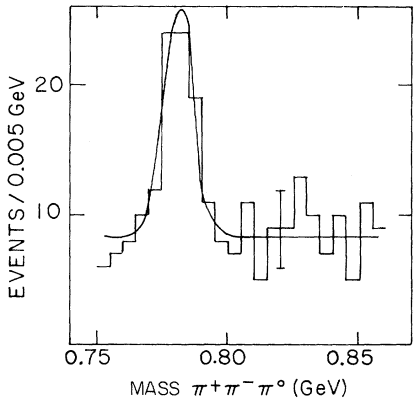

FIG. 4. The MM spectrum for events satisfying the hypothesis $\pi^-p \to \pi^+\pi^-\pi^0 n$. The data have been fit to a constant plus a Gaussian ω.

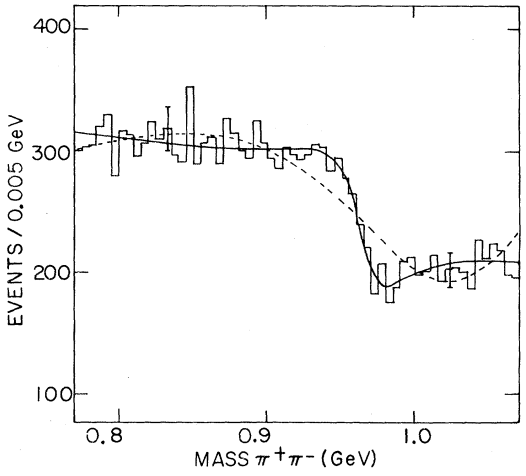

FIG. 5. The MM spectrum for events from the reaction $\pi^-p \to \pi^+\pi^-n$ where only one pion reaches the spectrometer. The solid curve is the best S^* fit to the data as described in the text. The dashed curve is the best fit if the nonresonant s-wave phase is held at 90°.

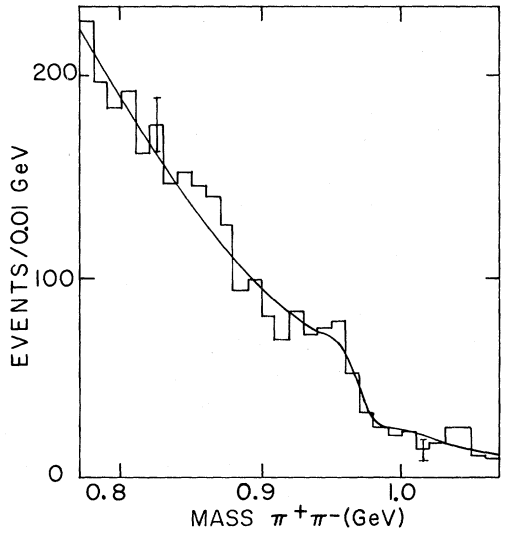

FIG. 6. The MM spectrum for $\pi^-p \to \pi^+\pi^-n$ where one pion is momentum analyzed and the second has only an angles measurement in the spectrometer. The curve is the best S^* fit.

important. The successfully detected events by constraint class were then transformed into the X^0 rest frame (RF, the Gottfried-Jackson frame was used.) For our highly peripheral events, the Lorentz transformation to and the polar axis of the RF are essentially along the beam direction. The 4C events were found to populate a π^+ polar angle θ region near 90° in the X^0 RF. After transformation into the laboratory frame, the two mesons are forward going and nearly symmetric with respect to the beam line. This condition ensures two trajectories which pass through the spectrometer. The detection efficiency drops as the transverse momentum increases which means that the acceptance falls with MM at a given RF polar angle. The 1C events are produced with the π^+ either parallel or antiparallel to the beam direction. This gives one particle through the spectrometer while the second misses altogether. The acceptance for 1C events is nearly MM independent. The 3C acceptance is intermediate between the other two classes in angle. It falls with MM although more slowly than the 4C acceptance. An important point is that we accept one- and three-constraint events independent of the polarity of the analyzed trajectory. This gives acceptances which are symmetric about $\theta = 90°$ in the RF.

Efficiencies were also generated for nonzero-X^0-spin states. The general result is that spin-projection-zero states, whose angular distributions peak near $\theta = 0°$ and 180°, tend to populate the 1C class, whereas nonzero projections are more important to the 3C class. One effect of this may be seen in the absence of ρ from the 1C data where the spin-projection-zero–production differential cross section has been observed to dip near $t = t_{\min}$.[5]

For the analysis presented in this paper, only the acceptance versus MM obtained by integrating over RF angles is needed. After integration, the acceptance for 1C events is MM independent to within 10%, whereas the 3C acceptance is a decreasing function of MM. This accounts for the largest part of the difference between the data in Figs. 5 and 6. Other contributions to the experimental acceptance are at worst slowly varying functions of MM. As will be demonstrated later, any weak dependence of the acceptance or backgrounds on MM does not bias the S^* parameters which are determined by the sharp edge in the data. Two specific mass dependences which are demonstrably weak in this context are the ρ Breit-Wigner and foreseeable s-channel effects. Indeed it is the sharpness of the S^* shoulder relative to such effects which permits, within the framework of the model used, an extraction of the s-wave parameters.

III. ANALYSIS

The analysis procedure we use is minimization of the χ^2 for the hypothesis that the mass spectra in Fig. 5 and 6 are of the form

$$\frac{dN_c(M)}{dM} = J(M)F(t,M)[\epsilon_c^0(M)\,|\,T_\pi^0(M)|^2 + \epsilon_c^1(M)|T_\pi^1(M)|^2] + B_c(M). \tag{4}$$

$dN_c(M)$ is the number of events of constraint class c in the missing-mass interval dM. $J(M)$ is the solid angle subtended by the neutron counters in the over-all center-of-mass frame multiplied by a normalization constant. ϵ_c^0 is the s-wave Monte Carlo efficiency for constraint class c; T_π^0 is the s-wave $\pi\pi$ scattering amplitude. ϵ_c^1 and T_π^1 are the corresponding p-wave functions. We have tried fits including corresponding d-wave functions in the form of the f meson and have found their contribution to be consistent with zero. Note that Eq. (4) implicitly assumes that an integration over angles (in the RF) has been performed. The cross term between s and p waves cancels in this integration because our detection efficiency is symmetric about 90°.

The factor $F(t,M)$ describes all of the dynamics of the reaction except for the $\pi\pi$ scattering term which is explicitly factored out. The form of F is not known; however, we find from our analysis that the S^* parameters are independent of the form of F provided it is only a slowly varying function of M. Specifically we have performed separate analyses of 1C $\pi^+\pi^-n$ data using a one-pion exchange form for F[5] and using the form $\exp(7t_{\min})$. We have also analyzed with the product $F(t,M)$ $J(M)$ set equal to a constant. Neither the s-wave cross section nor the over-all quality of our fits (χ^2 probability) is a function of the choice among these three options. The results to be presented were obtained using the one-pion exchange form for F.

We parameterize the s-wave amplitude by[9,10]

$$T_\pi^0(M) = \frac{2}{3}\left[\frac{e^{2i\delta}-1}{2i} + \frac{e^{2i\delta}\Gamma_\pi M_0}{M_0^2 - M^2 - iM_0(\Gamma_\pi + \Gamma_K)}\right],$$

$$\Gamma_\pi = g_\pi(\tfrac{1}{4}M^2 - m_{\pi^+}{}^2)^{1/2},$$

$$\Gamma_K = g_K[(\tfrac{1}{4}M^2 - m_{K^+}{}^2)^{1/2} + (\tfrac{1}{4}M^2 - m_{K^0}{}^2)^{1/2}]. \tag{5}$$

Here δ, M_0, g_π, and g_K are the adjustable parameters; m_{π^+}, m_{K^+}, and m_{K^0} are the masses of the π^+, K^+, and K^0. Γ_K is the sum of the partial widths for decay to the final states $K^+K^-(\Gamma_{K^+})$ and $K^0\bar{K}^0(\Gamma_{K^0})$. Below $K\bar{K}$ thresholds the positive imaginary square root is implied. The final objective of our analysis, the position of the S^* pole,

is by definition the complex zero of the denominator of the second term of $T_\pi^0(M)$.

For the p-wave contribution either we use a ρ Breit-Wigner multiplied by the Monte Carlo-generated efficiency, or we include the p-wave effects in the background term $B_c(M)$. The former case will be referred to as the physical background, the latter as the polynomial background. For the physical background the ρ amplitude is a parameter and $B_c(M)$ is taken to be a constant. In the polynomial background B is taken as a linear function of M for 1C data and a quadratic function for 3C data. The final form of Eq. (4) contains either seven or eight adjustable parameters: the over-all normalization, four s-wave parameters and two or three background parameters. We find that not all the s-wave parameters can be determined from the $\pi^+\pi^-n$ data. The reason is illustrated in Table I where fits are made to the 1C $\pi^+\pi^-n$ data after fixing g_K at various values. We obtain excellent fits independent of g_K. In fact, the $\pi^+\pi^-n$ data by themselves are consistent with the hypothesis $g_K = 0$ which implies no coupling to the $K\bar{K}$ system. The remaining parameters of the s-wave amplitude are strong functions of g_K, but if one extracts the position of the S^* pole, it is nearly independent of g_K. Our procedure then is to fix g_K, fit our two data sets to the expression in Eq. (4), and extract the pole parameters. We then fit our K^+K^-n data as will be described later to find g_K.

We have already noted the independence of the pole position on the form of $F(t,M)$. To check its dependence on background we list in the first four rows of Table II the pole position from fits made to the data in Figs. 5 and 6 using the physical and polynomial backgrounds. The χ^2 probabilities for the various fits are given in column 4 of Table II. The 1C fits are excellent and the 3C fits are acceptable. The fits from rows 1 and 2 are shown as the solid curves in Figs. 5 and 6, respectively. There is an obvious consistency between fits to the two data classes and an independence from the background parameterization. The computed pole position is found to be independent of the form of the background within the computed errors. We have tried other fits, among them higher-order polynomial backgrounds, with equivalent results. The pole parameters display an independence from the RF decay angles since the two data classes sample different angular ranges. The over-all normalizations are also consistent within errors which serves to check the Monte Carlo efficiencies. For example, for the two physical background fits, the normalizations are 578 ± 37 and 640 ± 67.

To complete the analysis we fit the sample of 4C K^+K^-n data shown in Fig. 7. The fitting function used was[10]

$$\frac{dN_K}{dM} = F(t,M)\,J(M)\epsilon_K^0(M)\,|T_K^0(M)|^2, \qquad (6)$$

$$T_K^0(M) = \frac{M_0(\Gamma_\pi\Gamma_{K^+})^{1/2}/\sqrt{3}}{M_0^2 - M^2 - iM_0(\Gamma_\pi + \Gamma_K)}.$$

Equation (6) is the analog of Eqs. (4) and (5) with p wave omitted and the s-wave amplitude replaced by the inelastic amplitude T_K^0 for the process $\pi^+\pi^- \to K^+K^-$. The efficiency $\epsilon_K^0(M)$ is the Monte Carlo generated K^+K^- acceptance. In fitting with this function we hold the S^* pole at the value given above from the $\pi^+\pi^-$ fits. We hold the over-all normalization at the $\pi^+\pi^-$ value. This leaves one free parameter, g_K. Because of nonzero M resolution there are some K^+K^-n events below threshold. To analyze these data it is necessary to include our $\sigma = 4$-MeV/c^2 resolution in the fit.[11] Likewise even a small mass shift can affect the fits enormously. We have already observed that the mass of our ω signal is 2 MeV/c^2 low. We also find that the K^+K^- threshold is 3 MeV/c^2 low.

TABLE I. Table I demonstrates the independence of the S^* pole position (as calculated from the $\pi^+\pi^-n$ 1C data) from the parameter g_K. Each row gives results from a fit with g_K assigned the value in column 1. Column 2 gives the χ^2 probability of the fit, while columns 3 through 5 give the remaining s-wave parameters. Column 6 shows that the pole is a very weak function of g_K and may even be found for $g_K = 0$.

g_K	χ^2 probability (%)	g_π	M_0 (MeV/c^2)	s-wave background phase (degrees)	Pole position (MeV/c^2)
2.5	95	0.71 ± 0.14	745 ± 23	61 ± 6	$(971 \pm 5) - i(23 \pm 5)$
0.5	97	0.20 ± 0.04	917 ± 8	62 ± 5	$(971 \pm 5) - i(22 \pm 5)$
0.25	95	0.15 ± 0.03	942 ± 6	61 ± 5	$(967 \pm 5) - i(22 \pm 5)$
0.06	94	0.11 ± 0.02	959 ± 4	57 ± 5	$(965 \pm 5) - i(21 \pm 5)$
0	93	0.09 ± 0.02	964 ± 4	55 ± 4	$(964 \pm 5) - i(21 \pm 5)$

TABLE II. The results in Table II demonstrate the independence of the S^* pole position (column 6) and s-wave background phase (column 5) from the form used to parameterize background in the χ^2 fit. Each row of the table represents a separate fit. Column 1 lists the constraint class used, column 2 the mass range of the fit, and column 3 the background form as described in the text. Column 4 is the χ^2 probability of the fit.

Constraint class	Mass range (MeV/c^2)	Background form	χ^2 probability (%)	s-wave background phase (degrees)	Pole position (MeV/c^2)
1C	770–1070	Linear	94	57 ± 5	$(965 \pm 5) - i(21 \pm 5)$
3C	770–1070	Quadratic	9	49 ± 14	$(970 \pm 6) - i(13 \pm 6)$
1C	770–1070	Physical	94	57 ± 5	$(966 \pm 4) - i(21 \pm 4)$
3C	770–1070	Physical	2	51 ± 7	$(972 \pm 6) - i(24 \pm 5)$
1C	890–1015	Constant	86	59 ± 9	$(973 \pm 6) - i(26 \pm 5)$
3C	900–1015	Constant	87	35 ± 14	$(962 \pm 10) - i(27 \pm 7)$

After compensating for this shift we obtain the 75% confidence-level fit shown in Fig. 7 for $g_K = 0.25 \pm 0.05$. The values for g_π, M_0, and δ are found by refitting the $\pi^+\pi^- n$ 1C data with a 3-MeV/c^2 mass shift and $g_K = 0.25$. The resultant values are $g_\pi = 0.14 \pm 0.03$, $M_0 = 943 \pm 6$ MeV/c^2, and $\phi = 60° \pm 5°$. From these results, the position of the S^* pole is $(970 \pm 5) - i(22 \pm 5)$ MeV/c^2, on the second sheet.

Our nonresonant s-wave background phase is markedly different from previous observations which have either been near 90°[3] or near 0°.[4] Likewise, the real part of our S^* pole position is approximately 20 MeV/c^2 below the world average.[1] We do observe from our fits that the position of the S^* pole is correlated with the background phase. If we fix the background phase at 90° in agreement with Ref. 3, the best fit is shown as the dashed curve in Fig. 5. The quality of the fit suffers as the fitting function is no longer able to reproduce the sharpness of the S^*. The pole moves to $(996 \pm 2) - i(35 \pm 6$ MeV/c^2 giving a real part of the pole position in agreement with the world average and an imaginary part too large by a factor of 2.

A possible explanation of the discrepancy between our pole position and the world average would be the inadequacy of our model which holds the background phase constant over our entire mass range. However, fits over a restricted mass range (rows 5 and 6 of Table II) show that the best-fit background phase does not change when data far from the S^* edge are eliminated. A background phase substantially below 90° is required to match the data near 950 MeV/c^2. A slow variation in this phase at other masses could be absorbed in the background terms from higher partial waves. These results still hold for fits to even smaller mass ranges although the parameter errors become large rapidly.

IV. CONCLUSIONS

Previous to the results reported in this paper there have been three high-precision measurements of the S^* pole position, z.[4–6] All three are consistent among themselves and with our result for Im(z). Two of the measurements, Binnie *et al.*,[4] and Protopopescu *et al.*,[6] report significantly greater precision in their determination of Re(z) than does the third.[5] Binnie *et al.* report Re(z) = 987 ± 7 MeV/c^2 based on fits to the dipion mass spectrum for the reaction $\pi^- p \to \pi^0\pi^0 n$ at threshold. Interestingly, they find Re(z) = 977 for the reaction $\pi^- p \to \pi^+\pi^- n$ at threshold, but this data sample has a poor signal-to-noise ratio and was

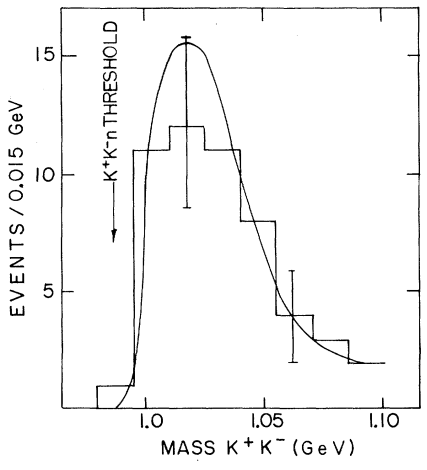

FIG. 7. The MM spectrum for $\pi^- p \to K^+ K^- n$ with both kaons momentum analyzed in the spectrometer. The curve is a one-parameter (g_K) fit to the data with the S^* pole held at the $\pi^+\pi^- n$ best value.

disregarded. In both cases the background phase is taken to be 0°. Protopopescu *et al.* find $\mathrm{Re}(z) = 997 \pm \mathrm{MeV}/c^2$ in a partial-wave analysis of the reaction $\pi^+ p \to \Delta^{++}\pi^+\pi^-$ at 7.1 GeV/c. The same group in an earlier analysis of their data[3] quote a background phase near 90°. The weighted average of previous results[1] is $z = (993 \pm 4) - i(20 \pm 4)$ MeV/c^2 compared to our result $z = (970 \pm 5) - i(22 \pm 5)$ MeV/c^2.

ACKNOWLEDGMENTS

We wish to thank the staff of the ZGS for their support. Special thanks are due to Drs. R. Diebold, D. Ayres, S. Kramer, B. Wicklund, I. Ambats, and the remaining members of the EMS group. We acknowledge the contributions of P. Hornung, M. Anderson, and R. Boz at various stages in the experiment.

---

†Research supported by the U. S. Energy Research and Development Administration under Contract No. W-7405-eng-82.

‡Present address: Sandia Laboratory, Division 5245, Albuquerque, New Mexico 87115.

‖Present address: Department of Physics and Astronomy, University of Rochester, Rochester, N. Y. 14527.

[1]A complete set of references may be found in Particle Data Group, Phys. Lett. 50B, 1 (1974).

[2]M. Alston-Garnjost *et al.*, Phys. Lett. 36B, 152 (1971).

[3]S. M. Flatte *et al.*, Phys. Lett. 38B, 232 (1972).

[4]D. M. Binnie *et al.*, Phys. Rev. Lett. 31, 1534 (1973).

[5]B. Hyams *et al.*, Nucl. Phys. B64, 134 (1973); P. Estabrooks *et al.*, in π-π *Scattering—1973,* proceedings of the International Conference on π-π Scattering and Associated Topics, Tallahassee, 1973, edited by P. K. Williams and V. Hagopian (A.I.P., New York, 1973).

[6]S. D. Protopopescu *et al.*, Phys. Rev. D 7, 1279 (1973).

[7]M. Buttram *et al.*, Phys. Rev. Lett. 35, 970 (1975).

[8]D. S. Ayres, ANL Report No. ANL/HEP 7314, 1973 (unpublished).

[9]For the purpose of locating the S^* pole the exact form of T_π^0 is not crucial. For example, the amplitude

$$T_\pi^0 = Ae^{2i\delta} + \frac{\Gamma/2}{M_0 - M - i\Gamma/2},$$

where A, δ, M_0, and Γ are variable parameters (Γ is mass independent) gives a pole at $(967 \pm 6) - i(22 \pm 6)$ and a χ^2 probability of 93%. This amplitude unlike the one used in the text is not manifestly unitary.

[10]Our parameterization of the $\pi\pi$ scattering amplitude is very similar to that of Ref. 3. We differ only in the inclusion of the $K^0\bar{K}^0$ channel in the total width. Reference 4. uses the same width parameterization that we do, but employs a phase $\delta = 0$ and analyses in terms of mass rather than mass squared.

[11]We have studied the effect of the inclusion of resolution in our $\pi^+\pi^-n$ fits and found that the pole position is insensitive at the $\sigma = 4$ MeV/c^2 level. All the $\pi^+\pi^-n$ results presented in this paper were derived with resolution effects omitted.